Theory of frequency modulated thermal wave imaging for nondestructive subsurface defect detection

Ravibabu Mulaveesala and Suneet Tuli

Citation: Applied Physics Letters **89**, 191913 (2006); doi: 10.1063/1.2382738
View online: http://dx.doi.org/10.1063/1.2382738
View Table of Contents: http://scitation.aip.org/content/aip/journal/apl/89/19?ver=pdfcov
Published by the AIP Publishing

Theory of frequency modulated thermal wave imaging for nondestructive subsurface defect detection

Ravibabu Mulaveesala[a] and Suneet Tuli
Centre for Applied Research in Electronics, Indian Institute of Technology, Delhi New Delhi, India-110016

(Received 30 May 2006; accepted 20 September 2006; published online 10 November 2006)

This letter provides the theory and mathematical analysis in support of a recently proposed frequency modulated thermal wave imaging for nondestructive subsurface defect detection in solids. The authors illustrate how the technique simultaneously combines the advantages of both conventional pulse based thermography as well as modulated lock-in thermography. A specimen is heated for launching thermal waves into the sample, not at a single frequency (lock-in) or at all frequencies (pulse), but in a desired range of frequencies. While peak power requirement is reduced, phase images obtained retain known advantages. Experimental results from a carbon fiber reinforced plastic sample are presented in support. © *2006 American Institute of Physics*.
[DOI: 10.1063/1.2382738]

In recent years, thermal wave physics has played an important role in the area of nondestructive evaluation of subsurface defects in metallic, insulating, and composite materials. It is achieved by observing, recording, and analyzing the thermal response at the material surface to a heat stimulus, and is broadly known as active thermography in contrast to passive thermography where no heat stimulus is applied. Significant work has been done and understanding achieved in the propagation of thermal waves in materials and their reflection from subsurface features.[1]

Presently, two different approaches of active thermal nondestructive techniques are predominantly in use: pulsed thermography (PT) and modulated lock-in thermography (LT).[1–4] In pulse thermography, the tested material is warmed or cooled with a short duration energy pulse (for example, optical, induction heating, and ultrasonic heating, etc.) and a measurement of the temporal evolution of the surface temperature is performed with an infrared (IR) camera. The surface temperature gradients on the sample help to localize the defects inside the material. However, the surface temperature gradients are not only caused by hidden defects but also affected by local variations of emissivity on the material surface as well as due to nonuniform heating. Lock-in thermography uses periodic sinusoidal thermal excitation in order to derive information on reflected thermal wave phase and magnitude[4] even at considerably low peak powers. The phase angle has the advantage of being less sensitive to local variations of illumination and/or of surface emissivity. Because of its monofrequency excitation, the depth resolution of a test is fixed (i.e., fixed "thermal wavelength"). To detect defects located at various depths in the test sample, repetition of the test at various frequencies becomes a time consuming process. Experimental arrangement for another technique, pulsed phase thermography (PPT),[2,3] is similar to that of PT, but the image sequence captured during the experiment is processed differently. In PPT, the extraction of various frequency components present is performed by Fourier transform on each pixel of the thermal image sequence.[3] The phase images thus obtained show all the merits of the phase images obtained with LT.[4] To overcome some of the traditional limitations of conventional thermal wave imaging techniques (resolution, peak power, depth of penetration), the present work focuses on nonstationary forms of thermal excitation technique: frequency modulated thermal wave imaging.[5–8] A physical insight based on mathematical analysis of the underlying thermal wave process is provided.

The model for studying thermal waves is based on the equation of heat flow due to conduction, which in a one-dimensional case (in the absence of heat sources and sinks) is given as follows;[9]

$$\frac{\partial^2 T(x,t)}{\partial x^2} = \frac{1}{\alpha}\frac{\partial T(x,t)}{\partial t}, \tag{1}$$

where $T(x,t)$ is the temperature, $\alpha = k/\rho c$ is the thermal diffusivity, k is the thermal conductivity, ρ is the density, and c is the specific heat. The space coordinate is x and t is time.

The solution for the $T(x,t)$ is obtained after taking into account the boundary conditions at the irradiated sample surface ($x=0$) and the opposite face ($x=d$), with $d \to \infty$ in case of semi-infinite solid. In thermal wave imaging a common technique to generate thermal waves is through absorption of incident sinusoidal intensity modulated light beam at the surface $x=0$.

The expression for $T(x,t)$ can be written in terms of real and imaginary parts,

$$T(x,t) = T_0 e^{-x\sqrt{\pi f/\alpha}}[\cos(\kappa) + j\sin(\kappa)]. \tag{2}$$

$$\kappa = 2\pi f t - x\sqrt{\frac{\pi f}{\alpha}}. \tag{3}$$

Equation (2) shows the resultant temperature distribution caused by the wavelike propagation of the heat flow into the bulk of the sample. Damping of the thermal waves as they propagate into the sample depends not only on the thermal properties of the sample but also on the frequency of incident heating. From Eq. (3), a thermal diffusion length μ, which is a measure of the depth probed by the thermal waves within the sample, can be written as follows:[1–3]

$$\mu = \sqrt{\frac{\alpha}{\pi f}}. \tag{4}$$

[a]Electronic mail: ravibabucareiitd@yahoo.co.in

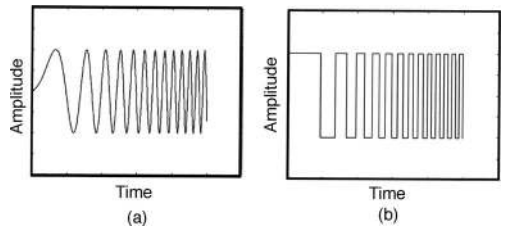

FIG. 1. (a) Linear frequency modulated signal and (b) its digitized form.

Unlike the case of sinusoidal intensity modulated surface heating of the sample, the proposed technique utilizes frequency modulated waves instead. Frequency modulated surface heat cycle of duration τ with a bandwidth B is obtained by means of linear frequency modulated heat flux [Fig. 1(a)] incident on the sample surface,

$$Q(x=0,t) = Q_0 e^{j2\pi(ft+Bt^2/2\tau)}. \tag{5}$$

The solution for the resulting temperature $T(x,t)$ from a such a modulated heating [Eq. (5)] can be derived to be

$$T(x,t) = T_0 e^{-x\sqrt{\pi/\alpha(f+Bt/\tau)}} e^{-jx\sqrt{\pi/\alpha(f+Bt/\tau)}} e^{2\pi j(ft+Bt^2/2\tau)}. \tag{6}$$

Further writing in terms of its real and imaginary parts,

$$T(x,t) = T_0 e^{-x\sqrt{\pi/\alpha(f+Bt/\tau)}} e^{j(2\pi(ft+Bt^2/2\tau)-x\sqrt{\pi/\alpha(f+Bt/\tau)})} \tag{7}$$

$$= T_0 e^{-x\sqrt{\pi/\alpha(f+Bt/\tau)}} [\cos(\kappa) + j\sin(\kappa)], \tag{8}$$

$$\kappa = 2\pi\left(ft + \frac{Bt^2}{2\tau}\right) - x\sqrt{\frac{\pi}{\alpha}\left(f + \frac{Bt}{\tau}\right)}. \tag{9}$$

The thermal diffusion length μ_{fm} in the case of frequency modulated heating can thus be written as

$$\mu_{\mathrm{fm}} = \sqrt{\frac{\alpha}{\pi(f+Bt/\tau)}}. \tag{10}$$

Here B/τ is the modulation factor of a linear frequency modulated signal, which controls the slope of frequency variation with time. The thermal diffusion length, being dependent on the bandwidth of the frequency modulated thermal excitation over the sample surface, helps to scan the entire depth of the sample with time during one frequency modulated cycle. If the modulation factor B/τ is zero, then the diffusion length formula becomes like that of Eq. (4), the special case of single frequency sinusoidal intensity modulated thermography (LT).

The thermal wave length (λ) in case of frequency modulated thermal wave imaging is given by

$$\lambda = 2\pi\mu = 2\pi\sqrt{\frac{\alpha}{\pi(f+Bt/\tau)}}. \tag{11}$$

Unlike in lock-in thermography, the wavelength in frequency modulated thermal wave imaging is not fixed but varies as a function of frequency during the experiment, leading to variation in the depth resolution for detection of defects at different depths.

An analog linear frequency modulated (chirp) incident heat flux $Q(x=0,t)$ [Fig. 1(a)] can be represented as in Eq. (5). Here Q_0 is the envelope of the chirp modulated incident heat flux, which is zero outside the time interval τ, and $\theta(t)=2\pi(ft+Bt^2/2\tau)$ is the phase of the chirp signal. The instantaneous frequency $f_m(t)$ of the chirp modulated incident heat flux can be obtained as follows:

$$f_m(t) = (1/2\pi)\frac{d\theta}{dt}. \tag{12}$$

The chirp rate represents the rate of change of instantaneous frequency, and is defined by

$$\gamma(t) = \frac{df_m}{dt} = (1/2\pi)\frac{d^2\theta}{dt^2}. \tag{13}$$

The waveform is said to be an up-chirp if $\gamma(t)>0$ and a down-chirp if $\gamma(t)<0$. It may be noted that $\gamma(t)=0$ signifies lock-in thermography.

Pulse thermography requires that enough energy be injected so that the returned signals from even deep defects are detectable. While the illuminating pulse duration is generally kept small, the peak power is conversely larger. This becomes a limitation for PT, but can be overcome by coded excitation in which instead of an increase in the peak power of the excitation signal, the average power is increased.[10] The fundamental concept of the digitally coded excitation system is shown in Fig. 1.

In digitized frequency modulated thermal wave imaging (DFMTWI) the input signal is clipped and converted into a binary (digital) form [Fig. 1(b)]. The digitized linear frequency modulated (digital chirp or square chirp) signal $Q_{\mathrm{dc}}(t)$ can be derived from its analog counterpart signal $Q(x=0,t)$ [Eq. (3)] by the nonlinear signum operation[6]

$$Q_{\mathrm{dc}}(t) = \mathrm{sgn}(Q(x=0,t)), \tag{14}$$

where

$$\mathrm{sgn}(Q(x=0,t)) = 1 \quad \text{when } Q(x=0,t) > 0, 0 \quad \text{when } Q(x=0,t) = 0, -1 \quad \text{when } Q(x=0,t) < 0.$$

The advantages of digitization of the analog chirp signal over the conventional analog form can be explained by comparing their spectra. While a simple sine wave has only one spectral component at a frequency $f(=\omega/2\pi)$, a square wave can be represented by its infinite Fourier series,

$$Q_{\mathrm{square}}(t) = \frac{4}{\pi}\sum_{b=0}^{\infty}\frac{1}{2b+1}\sin(2b+1)\omega t. \tag{15}$$

Computing root mean square values of sine and square, clear that the energy of a square wave is two times higher than the energy of the sine wave of the same amplitude. However, in a square wave the additional energy is due to higher harmonics, which do cause thermal waves inside the material but of amplitude levels which may be neglected. More energy is injected comparably at the fundamental frequency ($b=0$) in Eq. (15), which has an amplitude 1.273 ($=4/\pi$) times higher than the sine signal, leading to increased amplitude of reflected signal.

Experiments to validate the proposed DFMTWI technique were carried out on a carbon fiber reinforced plastic (CFRP) sample using a CEDIP IR (Jade MWIR, 3–5 μm) system. The CFRP sample made up of 30 layers, each having a thickness of 0.15 mm, also contains 15 numbers of square shaped Teflon inserts at every alternate layer from the sample

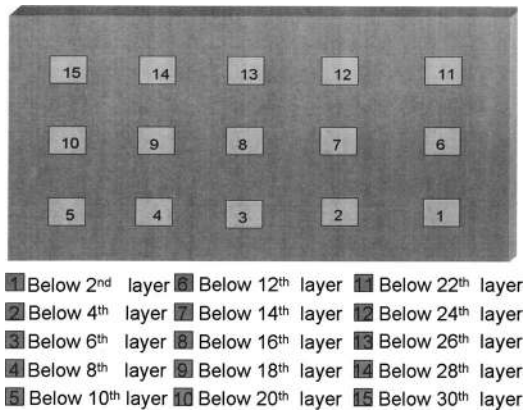

FIG. 2. Layout of the CFRP test sample with Teflon inserts at various depths. Teflon inserts are located every alternate layer of the 30 layered CFRP specimen ($265\times165\times4.5$ mm^3).

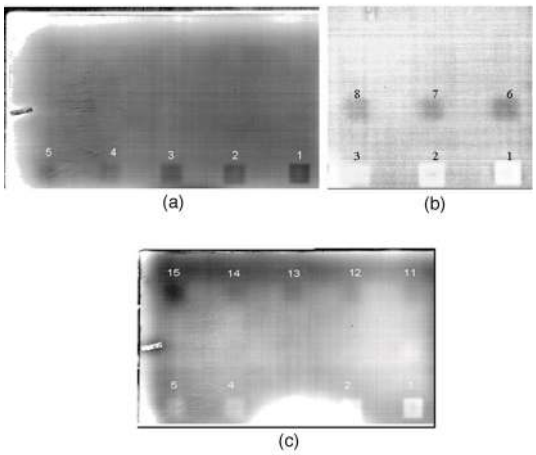

FIG. 3. Phase images of the CFRP sample with Teflon inserts, experimentally obtained using (a) 0.089 Hz, (b) 0.086 Hz, and (c) 0.001 Hz. Measurements are made over only one digitized frequency modulated cycle ($\tau=250$ sec, $B=0.01$ Hz).

top surface, as shown in Fig. 2. A digitized frequency modulated signal (digitized chirp) of 250 s duration, with frequency varying from 0.001 to 0.1 Hz, is generated from a signal generator and used to drive the heat sources (two halogen lamps with a power of 800 W each, placed about a meter away from the CFRP sample), via a source control unit. The advantage of digitized frequency modulated incident heat flux over the analog form is its simplicity of generation. However as in PPT,[3] computing the phase image reduces the associated effect considerably. The infrared camera observes the sample surface and records the temporal response of the sample by capturing a sequence of images during the digitized chirp heating. Various frequency components in captured sequence are extracted using the Fourier transform (F_n) on each pixel of the thermogram sequence containing N images. Let $T(k)$ be the temperature at a particular location of the kth thermogram in the image sequence ($0<k<N$). Then,

$$F_n = \sum_{k=0}^{N-1} T(k)e^{-2\pi ikn/N} = \mathrm{Re}_n + i\,\mathrm{Im}_n, \tag{16}$$

$$A_n = \sqrt{\mathrm{Re}_n^2 + \mathrm{Im}_n^2}, \tag{17}$$

$$\phi_n = \tan^{-1}\left(\frac{\mathrm{Im}_n}{\mathrm{Re}_n}\right). \tag{18}$$

Here Re and Im are the real and imaginary parts of the Fourier transform (FT). The subscript n denotes the frequency increments. The amplitude (A_n) and phase (φ_n) images are formed by repeating this process for all pixels in the frame.

Figures 3(a)–3(c) show the generated phase images of the CFRP sample, using DFMTWI at modulation frequencies of 0.089, 0.086, and 0.001 Hz, respectively. Experimental results illustrate the capability of DFMTWI to preserve the defect shape. Measurements were made over only one frequency-modulated cycle (0.001–0.1 Hz in 250 s) and the image sequence was captured at a frame rate of 20 Hz. For a fixed test frequency (as in LT), the thermal diffusion length [Eq. (4)] gets fixed and limits the depth resolution of the test. However, in digitized chirp heating the variable frequencies cause variable depth probing [Eq. (10)], with higher frequencies leading to lower depth of penetration and vice versa. In corroboration [Fig. 3(c)], the deepest row of defects (Teflon inserts 11–15 in Fig. 2), lying 3.75–4.5 mm below the front surface are clearly visible in the phase image obtained at the 0.001 Hz frequency. In the same figure, the shallowest defects (Teflon inserts 1–5 in Fig. 2) lying 0.3–0.75 mm below the surface are, however, not as clear as those obtained in the phase image [Fig. 3(a)], obtained at the higher frequency of 0.089 Hz. This is because generated thermal waves at lower frequencies have longer wavelengths causing poor resolution of near-surface defects. The phase image [Fig. 3(b)] at an in-between frequency, brings out the defects in intermediate layers (Teflon inserts 6–8). It may be noted that compared to PT, considerably less peak power is required from the heat sources for DFMTWI. Further, as compared to PPT, even though a much wider range of frequencies are probed simultaneously, higher order harmonics may not have sufficient energy to scan the test sample.

A potentially valuable thermal nondestructive testing technique has been proposed based on frequency modulated thermal waves, which combines the advantages of modulated (LT) and pulse thermography (PT and PPT) methods by probing the thermal waves into the test specimen in a desired range of frequencies and extracting the phase information from the observed thermal response. A theoretical basis has been provided for describing the proposed technique. Experiments have been carried out on the CFRP samples to detect the hidden Teflon patches at various depths, extending to 4.5 mm, in a single test.

[1]X. P. V. Maldague, *Theory and Practice of Infrared Thermography for Nondestructive Testing* (Wiley, Hoboken, NJ, 2001).
[2]J. R. Lhota, S. M. Shepard, B. A. Rubadeux, and T. Ahmed, Rev. Prog. Quant. Nondestr. Eval. **20A**, 492 (2000).
[3]X. Maldague and S. Marinetti, J. Appl. Phys. **79**, 2694 (1996).
[4]D. Wu and G. Busse, Rev. Gen. Therm. **37**, 693 (1998).
[5]R. Mulaveesala and S. Tuli, Insight **47**, 206 (2005).
[6]R. Mulaveesala and S. Tuli, Mater. Eval. **64**, 10 (2005).
[7]S. Tuli and R. Mulaveesala, *7th International Conference on Quantitative Infrared Thermography (QIRT) Proceedings*, 2004 (unpublished), Paper H.6.1.
[8]S. Tuli and R. Mulaveesala, Journal of Quantitative Infrared Thermography **2**, 41 (2005).
[9]H. S. Carlslaw and J. C. Jaeger, *Conduction of Heat in Solids* (Oxford University Press, London, 1959).
[10]Matthew O'Donnell, IEEE Trans. Ultrason. Ferroelectr. Freq. Control **39** (1992).